Miyata, K. Kangawa, T. Toshimori, T. Hatoh, H. Matsuo, *Biochem. Biophys. Res. Commun.* **129**, 248 (1985)]. Mass spectrometry of products from a nonradioactive labeling reaction was used to confirm the structure of iodinated Tyr^0-CNP.
21. The cells stably expressing the extracellular binding and transmembrane domains of ANPR-B that were used for binding studies express up to 1000 times more sites per cell than cells expressing the full-length receptor, either transiently in COS-7 cells or stably in 293 cells (*22*). This high degree of expression of the binding domain of the protein facilitated the subsequent binding assays by dramatically increasing the signal-to-noise ratio of the assay. [^{125}I]CNP binding isotherms on cells expressing the full-length ANPR-B or the truncated protein suggested that the affinity of CNP for both forms of the receptor was of a similar magnitude (*22*). Unfavorable signal-to-noise ratios for binding to intact ANPR-B precluded quantitative analysis.
22. D. G. Lowe *et al.*, unpublished observations.
23. It is possible that in other species, such as rat or pig, the natriuretic peptides may not display the same receptor preferences as in human. Similar studies on stimulation of the rat ANPR-A and ANPR-B guanylyl cyclases with CNP should help clarify this point. In addition, pBNP, which has some ability to stimulate human ANPR-B, may be a potent activator of the porcine ANPR-B.
24. M. Mukoyama *et al., N. Engl. J. Med.* **323**, 757 (1990).
25. A. McGregor, M. Richards, E. Espiner, T. Yandle, H. Ikram, *J. Clin. Endocrinol. Metab.* **70**, 1103 (1990).
26. J. N. Wilcox, A. Augustine, D. V. Goeddel, D. G. Lowe, in preparation.
27. J.-G. Chabot, G. Morel, R. Quirion, in *Current Aspects of the Neurosciences*, N. N. Osborne, Ed. (Macmillan, London, 1990), vol. 1, chap. 2.
28. P. Munson and D. Rodbard, *Anal. Biochem.* **107**, 220 (1980).
29. We thank C. Quan, M. Struble, and J. Burnier for peptide synthesis and purification; S. Wong for amino acid analysis; J. Bourell for mass spectrometric analysis; A. Renner for technical assistance; C. Morita, K. Andow, and L. Tamayo for help with computer graphics; and R. Vandlen for helpful discussions.

11 October 1990; accepted 23 January 1991

Spiral Calcium Wave Propagation and Annihilation in *Xenopus laevis* Oocytes

JAMES LECHLEITER, STEVEN GIRARD, ERNEST PERALTA, DAVID CLAPHAM*

Intracellular calcium (Ca^{2+}) is a ubiquitous second messenger. Information is encoded in the magnitude, frequency, and spatial organization of changes in the concentration of cytosolic free Ca^{2+}. Regenerative spiral waves of release of free Ca^{2+} were observed by confocal microscopy in *Xenopus laevis* oocytes expressing muscarinic acetylcholine receptor subtypes. This pattern of Ca^{2+} activity is characteristic of an intracellular milieu that behaves as a regenerative excitable medium. The minimal critical radius for propagation of focal Ca^{2+} waves (10.4 micrometers) and the effective diffusion constant for the excitation signal (2.3×10^{-6} square centimeters per second) were estimated from measurements of velocity and curvature of circular wavefronts expanding from foci. By modeling Ca^{2+} release with cellular automata, the absolute refractory period for Ca^{2+} stores (4.7 seconds) was determined. Other phenomena expected of an excitable medium, such as wave propagation of undiminished amplitude and annihilation of colliding wavefronts, were observed.

MANY G PROTEIN–LINKED RECEPTORS stimulate a common cell signaling pathway leading to activation of phospholipase C (PLC), release of diacylglycerol and inositol 1,4,5-trisphosphate (IP_3), and the subsequent IP_3-induced release of intracellular Ca^{2+} (*1*). The specificity of signal transduction by these receptors may be preserved by the spatiotemporal pattern of changes in the concentration of intracellular free Ca^{2+} ($[Ca^{2+}]_i$) (*2*). Consequently, we have examined such spatiotemporal patterns of release of free Ca^{2+} in the cytoplasm of *Xenopus* oocytes expressing muscarinic acetylcholine receptors (mAChRs), which are known to be coupled to turnover of phosphatidylinositol. The *Xenopus* oocyte is a valuable model for studying Ca^{2+} signaling. Changes in $[Ca^{2+}]_i$ have been followed by measuring the intrinsic Ca^{2+}-activated chloride ($I_{Ca,Cl}$) currents and by imaging with Ca^{2+}-sensitive dyes. Qualitatively different patterns of release of free Ca^{2+} have been observed in *Xenopus* oocytes, ranging from regenerative focal release to oscillations or propagating plane waves (*3, 4*). Several models have been proposed to explain the complex patterns of Ca^{2+} release. Oscillations in $[Ca^{2+}]_i$ may result from Ca^{2+}-induced Ca^{2+} release (CICR), while IP_3 remains constant, or from feedback mechanisms on PLC activity that cause IP_3 levels to vary (*5*). Since oscillatory $I_{Ca,Cl}$ currents have been observed in *Xenopus* oocytes with nonhydrolyzable analogs of IP_3 (*6*), the CICR hypothesis has recently gained factor.

Oocytes were used 48 hours after injection of mAChR transcripts (*4*) and were injected with the Ca^{2+} dye indicator fluo-3 (50 nl of 1 mM; ~50 μM final concentration) 30 to 120 minutes prior to each experiment. Confocal imaging of a single optical slice, close to the plasma membrane surface of each oocyte, was repeated at 1-s intervals. A two-electrode voltage clamp of $I_{Ca,Cl}$ was used in parallel with imaging to monitor Ca^{2+} release both within and distal to the imaging plane of the confocal microscope. As previously described, we found that the pattern of Ca^{2+} release induced by acetylcholine (ACh) was generally a propagating planar wave with velocities of 10 to 30 μm/s (*4*). This pattern of Ca^{2+} release was always accompanied by a rapid stimulation of $I_{Ca,Cl}$. In 14 of 30 oocytes, however, a more complex pattern of Ca^{2+} release was also observed—the occurrence of pulsating foci that produced circularly propagating Ca^{2+} waves. These regenerative patterns of Ca^{2+} release were observed at low ACh concentrations (10 nM) and at maximal ACh concentrations (1 to 50 μM), after the initial planar wave of Ca^{2+} had traveled through the imaging plane. At times, these regenerative waves of circular propagation would alter their pattern of propagation and change, from pulsating foci, into continuously cycling spiral waves of Ca^{2+} release (4 of 14 oocytes) (Fig. 1). The oocyte shown was stimulated with 1 μM ACh and exhibited the rapid $I_{Ca,Cl}$ current spike characteristic of mAChR responses (*4*). Approximately 2 min after ACh was applied to the oocyte, pulsatile focal Ca^{2+} release was observed and several of these foci developed into spiral waves. This complex pattern of Ca^{2+} release would not have been discerned in electrophysiological recordings alone, since the spatial information of Ca^{2+} release is not measured by the two-electrode voltage clamp method. Five images, captured over a 10-s period, followed the dominant spiral through one complete revolution (Fig. 1A). The spiral nature of the wave of Ca^{2+} release is more apparent when only the active wavefront is shown, as determined by sequential subtraction (*7*; Fig. 1, B and C). The initial wavelength, defined as the distance between the tangent of the spiral tip and the parallel tangent of the most adjacent wavefront, was ~210 μm.

The full regenerative character and the three-dimensional nature of spiral wave

J. Lechleiter, S. Girard, D. Clapham, Department of Pharmacology, Mayo Foundation, Rochester, MN 55905. E. Peralta, Department of Biochemistry and Molecular Biology, Harvard University, Cambridge, MA 02138.

*To whom correspondence should be addressed.

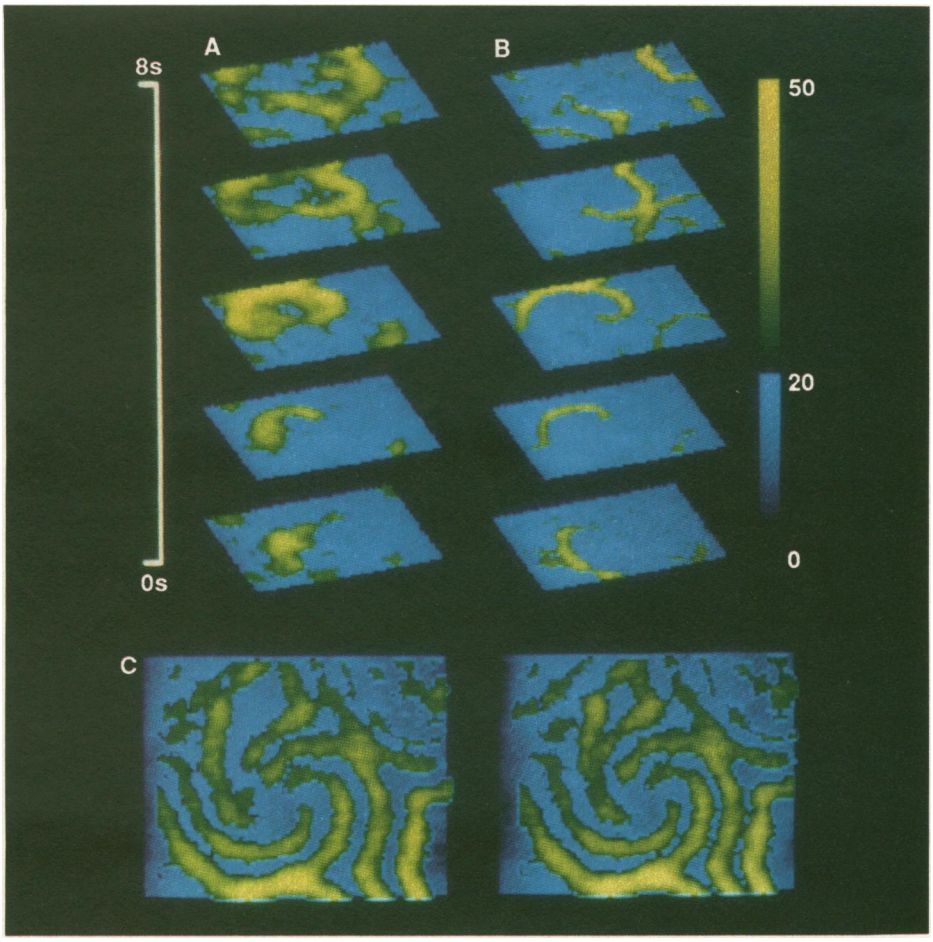

Fig. 1. Spiral Ca^{2+} wave propagation and annihilation. (**A**) Spatial patterns of Ca^{2+} release imaged at 2-s intervals at the surface membrane of the oocyte. This series of optical slices (650 by 650 by 40 μm) was recorded 2 min after the initial application of ACh (1 μM) in an oocyte expressing mAChRs. Resting concentrations of free Ca^{2+} are depicted on a blue scale. Increases in $[Ca^{2+}]_i$ are depicted in green-yellow, on the same scale (7). (**B**) Active wavefronts of Ca^{2+} release for the corresponding images shown in (A) determined by sequential subtraction (*7, 17*). (**C**) Stereo view (cross-fusion) of the five images shown in (B) observed normal to the *xy* plane of the oocyte. This view follows the completion of one period of spiral wave propagation (10 s). Note the annihilation of wavefronts when two propagating waves collide.

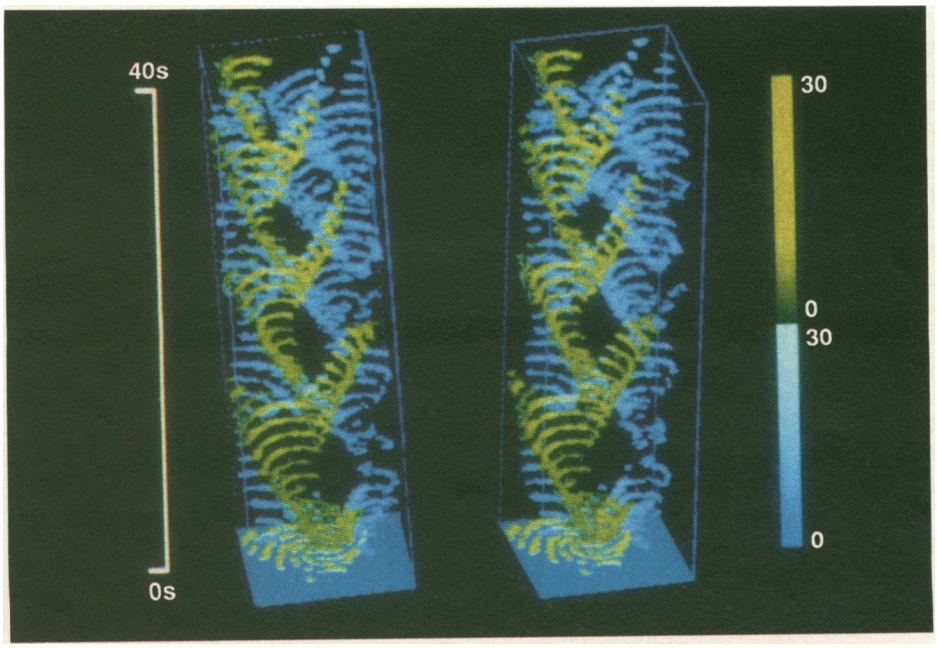

Fig. 2. Stereo projection of spiral wave activity, showing four periods. The three-dimensional image of Ca^{2+} wavefronts was created by sequentially subtracting and then stacking 40 consecutive images, captured at 1-s intervals (*7, 17*). The dominant spiral wave pattern is highlighted in green-yellow. All other wavefront activity is shown in blue. Ca^{2+} concentration scales are equivalent for blue and green-yellow intensity bars. The bottom optical slice is a normal projection of the green-yellow wavefronts (every other image) observed during the first period of propagation.

propagation are shown in Fig. 2 where four periods of activity are presented as a stereo pair. Although the pulsating foci that produced circular wavefronts were spatially stable, the foci of some spiral waves meandered. The focus of the dominant spiral in Fig. 2 (highlighted in green-yellow), for example, meandered ~50 μm over the 40-s period shown. Four minutes after application of ACh, the spiral wave patterns of Ca^{2+} release had subsided and planar waves were observed through this region of the oocyte. These observations indicated that there was no apparent structural basis, such as unusual formation of organelles, to account for the origin of this spiral activity. Another prominent feature of these Ca^{2+} release patterns was the mutual annihilation of colliding wavefronts (Figs. 1 and 2). Annihilation was independent of the type of wave propagation and was observed between planar, circular, and spiral waves. The absence of Ca^{2+} release in the wake of colliding waves observed here implied that the Ca^{2+} stores were refractory. However, the inability to release Ca^{2+} was only temporary, since the same region of an oocyte supported repetitive wave propagation (Fig. 2).

Our observations of wave propagation and annihilation suggest that the Ca^{2+} mobilizing machinery in the *Xenopus* oocyte behaves as an excitable medium. Excitable media are broadly defined as systems which, once excited by suprathreshold stimuli, must go through refractory periods before they are again competent to become excited (*8*). Wave propagation in excitable media was modeled by cellular automata [a cell is defined here as an individual Ca^{2+} store; (*9, 10*)]. Individual Ca^{2+} stores were spatially represented on an imaginary grid, each of which could be stimulated to release Ca^{2+} and interact with its neighbors during discrete time intervals (*11*). For each time iteration, an individual store was either releasing Ca^{2+} (defined as the excited state) or not releasing Ca^{2+} (defined as the relaxed state). A store does not release Ca^{2+} for one of two reasons; its Ca^{2+} concentration is too low or the store has not received sufficient

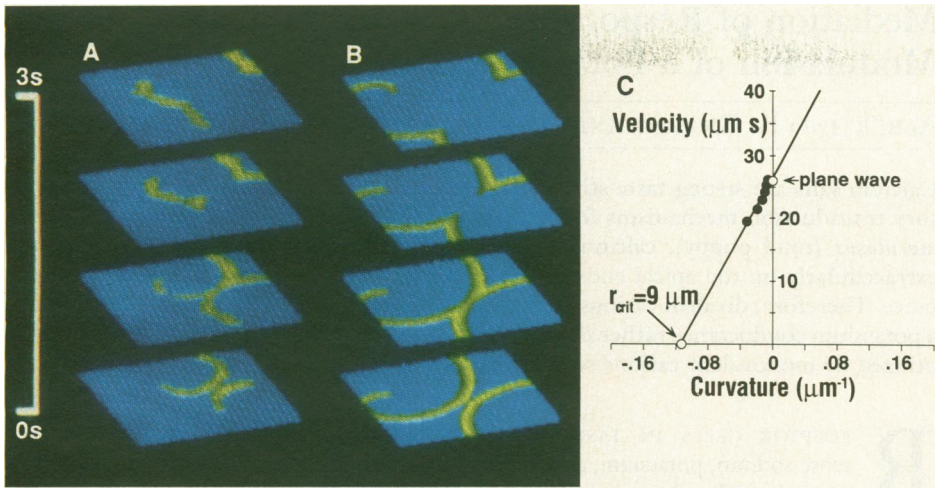

Fig. 3. Ca^{2+} release treated as an excitable medium. (**A**) Active Ca^{2+} wavefronts in an oocyte, propagating as a circular wave (lower right of each image) and a spiral wave (upper level) observed at 1-s intervals (*7, 17*). Resting $[Ca^{2+}]_i$ is shown in blue and increased $[Ca^{2+}]_i$ is portrayed in green-yellow. (**B**) Cellular automaton model for regenerative and refractory process. Initial conditions described a broken plane wave in the upper left-hand corner and a small focus in the lower right-hand corner. This model predicted an initial wavelength of 190 μm (the experimentally measured value was 210 μm) and an absolute refractory period of ~4.3 s (*11*). A second automaton model predicted a refractory time of ~4.2 s (*12*). (**C**) Plot of the wave velocity versus the curvature of Ca^{2+} wavefronts measured empirically from the radii of an expanding circular foci (*13*). The data, fit by a linear regression routine, predicted a critical radius for wave propagation of 9 μm.

stimuli from its neighbors. By modeling Ca^{2+} release with cellular automata, we estimated the refractory time of an individual Ca^{2+} store, a fundamental parameter related to the periodicity of the spiral wave propagation. The time per iteration and the unit length of an individual Ca^{2+} store were chosen to produce a model in which planar wave velocity and spiral period were equal to the observed values. The parameters were then adjusted until the predicted and the observed spiral wavelength converged. For four representative spiral waves, from four different oocytes, the model predicted wavelengths of 196, 122, 180, and 150 μm compared to measured values of 210, 125, 162, and 140 μm. The cellular automaton model of Ca^{2+} release, given the appropriate parameters and initial conditions (*11*), reproduces the observed behavior, including the annihilation of colliding wavefronts (Fig. 3B). The refractory time of an individual Ca^{2+} store, estimated from this model, was 4.7 ± 1.4 s (mean ± SD, n = 4). This value agreed with the prediction from a second, independent automaton (*12*).

Elementary theory of excitable media predicts that the speed of a propagating wavefront decreases in proportion to the curvature of the wavefront (*8*). For small curvatures, a linear relation between the curvature of the propagating wavefront and its normal velocity is predicted (*13*). We plotted the radii of expanding, circular wavefronts against time, numerically differentiated a third-order polynomial best fit to this graph, and determined the velocity at a given radius of curvature (Fig. 3C). The slope of this plot represents the effective diffusion coefficient of the excitable signal (*13*). The mean diffusion coefficient was 2.3 ± 0.78 × 10^{-6} cm^2/s (mean ± SD, n = 4). This coefficient is closer to the rate of diffusion of Ca^{2+} within cells (4.0 × 10^{-6} cm^2/s) (*14*) than to estimates of the diffusion coefficient of IP_3 [3.3 × 10^{-7} cm^2/s; (*15*)], thus tentatively supporting CICR as the dominant mechanism for Ca^{2+} wave propagation. Finally, theory also predicts a critical radius of excitation, below which propagation is not possible (*16*). An upper limit of this radius was estimated by extrapolating the linear relation between wavefront curvature and speed of propagation to zero velocity. The critical radius for Ca^{2+} propagation in our oocytes was 10.4 ± 3.2 μm (mean ± SD, n = 4). These data suggest that a suprathreshold quantity of Ca^{2+}, IP_3, or both is necessary to trigger regenerative Ca^{2+} release.

Propagation and annihilation of spiral Ca^{2+} waves is an example of spontaneous spatiotemporal organization in biological systems. When these and other complex patterns of Ca^{2+} released in stimulated oocytes are modeled as an excitable medium, important parameters can be derived that should help to define the underlying processes. Further experiments are necessary to clarify the specific roles of CICR and IP_3 in these regenerative processes, to identify the source of the critical radius for excitation, and to elucidate the nature of the Ca^{2+} stores in this model system.

REFERENCES AND NOTES

1. M. J. Berridge and R. F. Irvine, *Nature* **341**, 197 (1989).
2. M. J. Berridge, P. H. Cobbold, K. S. R. Cuthbertson, *Philos. Trans. R. Soc. London Ser. B* **320**, 325 (1988); T. Cheek, *J. Cell Sci.* **93**, 211 (1989); M. J. Berridge, *J. Biol. Chem.* **265**, 9583 (1990).
3. W. B. Busa *et al.*, *J. Cell Biol.* **101**, 677 (1985); I. Parker and R. Miledi, *Proc. R. Soc. London Ser. B* **228**, 307 (1986); I. Parker and R. Miledi, *ibid.* **232**, 59 (1987); H. Y. Kubota *et al.*, *Dev. Biol.* **119**, 129 (1987); M. J. Berridge, *Proc. R. Soc. London Ser. B* **238**, 235 (1989); G. Brooker *et al.*, *Proc. Natl. Acad. Sci. U.S.A.* **87**, 2813 (1990).
4. J. Lechleiter *et al.*, *EMBO J.* **9**(13), 4381 (1990); J. Lechleiter, S. Girard, D. Clapham, E. Peralta, *Nature*, in press. Oocytes were injected with mAChR transcripts encoding either m3 or Hy19 subtypes (Hy19 is a hybrid mAChR with receptor properties that are indistinguishable from m3 receptors; references herein).
5. N. M. Woods *et al.*, *Nature* **319**, 600 (1986); K. Swann and M. Whitaker, *J. Cell Biol.* **103**, 2333 (1986); T. Meyer and L. Stryer, *Proc. Natl. Acad. Sci. U.S.A.* **85**, 5051 (1988); I. Parker and I. Ivorra, *ibid.* **87**, 260 (1990); A. Goldbetter, G. Dupont, M. J. Berridge, *ibid.*, p. 1461; N. Dascal and R. Boton, *FEBS Lett.* **267**, 22 (1990).
6. M. Wakui *et al.*, *Nature* **339**, 317 (1989); C. W. Taylor, M. J. Berridge, A. M. Cooke, B. V. L. Potter, *Biochem. J.* **259**, 645 (1989); S. Delisle, K. Krause, G. Denning, B. V. L. Potter, M. J. Welsh, *J. Biol. Chem.* **265**, 11726 (1990).
7. All images (256 intensity levels, 128 by 128 pixels) were captured at 1-s intervals and analyzed after low pass filtration (9 by 9 sigma filter, σ = 20). One optical slice, prior to agonist application, was arbitrarily chosen to represent the resting $[Ca^{2+}]_i$ image (blue pixels). No change in resting $[Ca^{2+}]_i$ was observed without the addition of ACh. Increases in $[Ca^{2+}]_i$ (green-yellow pixels) were obtained by subtracting the resting $[Ca^{2+}]_i$ image from each of the consecutive optical slices. Active wavefronts of increases in $[Ca^{2+}]_i$ were obtained by subtracting from each optical slice the image immediately preceding it. For final display, the images of increased $[Ca^{2+}]_i$ were overlaid on the image of the resting $[Ca^{2+}]_i$. At the image locations where green-yellow and blue pixels overlap, only the increase in $[Ca^{2+}]_i$ is shown. Increases in $[Ca^{2+}]_i$ of less than 2 units were not plotted. This did not affect the peak magnitude of increases in $[Ca^{2+}]_i$, but highlighted the patterns of Ca^{2+} release. All Ca^{2+} concentrations are presented as absolute units, ranging from 0 to 255. An in vitro calibration (*4*) placed 0 to 20 units between 10 and 40 nM Ca^{2+} with the maximum intensity of 255 corresponding to more than 300 nM Ca^{2+} (A. B. Harkins, N. Kurebayashi, S. Hollingworth, S. M. Baylor, *Biophys. J.*, **59**, 240a, 1991). Images were collected with a Lasersharp MRC-600 Bio-Rad confocal box adapted to an IM35 Zeiss microscope (Zeiss 10× F achromat objective, 0.25 NA) and analyzed with ANALYZE software (Mayo Foundation, Rochester, MN) on a Silicon Graphics, Personal Iris computer. The confocal detector aperture was set at the largest opening, 7 mm, and the photomultiplier gain was set at the maximum. The optical thickness was estimated by the tilted reflector method (Bio-Rad technical bulletin).
8. A. T. Winfree, *Science* **175**, 634 (1972); *When Time Breaks Down* (Princeton Univ. Press, Princeton, NJ, 1987); *Ann. N.Y. Acad. Sci.* **591**, 190 (1990).
9. M. Gerhardt *et al.*, *Science* **247**, 1563 (1990).
10. M. Markus and B. Hess, *Nature* **347**, 56 (1990).
11. Cellular automaton and notation (*9*) was used with a 100 by 100 grid of Ca^{2+} stores and a 7 by 7 neighborhood, with the radius, r = 3. The variable ν, representing the degree of excitability of a Ca^{2+} store, was used to calculate the threshold of stimuli needed for excitation. For maximal excitability (defined here as a fully loaded Ca^{2+} store) we set ν = 0. We set the maximum value of ν (defined here as a fully depleted Ca^{2+} store) to ν_{max} = 100; the recovery threshold to ν_{rec} = 90; the excitation threshold to ν_{exc} = 35. During each time iteration,

the value of v increased in discrete integer steps (g_{up}) for excited stores and decreased by discrete integer steps (g_{down}) for recovering stores. We set $g_{up} = 25$ and $g_{down} = 5$. In the equation $\{k_{co}+[r\ (2r + 1) - k_{co}]\ (v/v_{exc})\}$, $k_{co} = 5$ was used to calculate the minimum number of excited neighbors necessary to excite a resting store at v; $k_{ro} = 7$ was used in the equation $\{k_{ro} + [r(2r + 1) - k_{ro}]\ [(v - v_{max}) / (v_{rec} - v_{max})]\}$ to calculate the minimum number of relaxed neighbors to cause relaxation of an excited store at v. At time zero, a 20 by 20 square of stores was excited ($v = 0$) next to a 20 by 20 recovering square of stores ($v = v_{max}$). This resulted in a stable spiral that had an initial wavelength of 56 stores and a period of 25 iterations. When a single row of stores was stimulated, the plane wave velocity was three stores per iteration. Given the empirically measured spiral period of 10 s and a plane wave velocity of 26 μm/s, this model predicted 0.4 s per iteration and 3.4 μm per store. The predicted initial wavelength of 190 μm differed by less than 10% from the observed value. The predicted minimum refractory time, $(v_{rec} - v_{exc})/g_{down}$, was 4.3 s.

12. The automaton presented by Markus and Hess (*10*) was also used to model spiral waves. In this model each Ca^{2+} store was described only by its state variable, S. Upon excitation, a store goes from its ground state $S = 0$ (fully loaded Ca^{2+} store) to the excited state $S = n + 1$ (partially depleted Ca^{2+} store). Thereafter, S decreases by 1 with each iteration. A store was refractory (could not release Ca^{2+}) when S was between S_{max} and n. A store was activated when S was between 0 and S_{max} and when a sufficient number of neighbor stores, within a circle of radius r, were excited. The expression, $m_0 + pS$, described the linear relationship between S and the threshold number of excited neighbors necessary for excitation. Thus, at $S = 0$, m_0 excited neighbors were needed for excitation. The following parameters were used to model the spiral wave: a 50 by 50 grid of Ca^{2+} stores, $r = 4$, $m_0 = 1$, $S_{max} = 4$, $p = 2$, $n = 6$. The velocity of a plane wave, initiated by activating one edge of the grid, was 3.4 stores per iteration. A broken plane wave was used to initiate a spiral that had a period of 7 iterations, and an initial wavelength of 18 stores. When the period of the automaton was set to the experimentally observed value of 10 s, one iteration corresponded to 1.4 s. By equating the automaton's plane velocity to 26 μm/s, one store unit was calculated to be 10.8 μm. The predicted initial wavelength of this automaton (195 μm) differed by less than 8% from the observed value (210 μm). The refractory period, determined from the algorithm of the automaton, $(n + 1 - S_{max})$, was 4.2 s.
13. The linear relation, $N = c - DK$, where N is the normal velocity, c is the planar wave velocity, D is diffusion constant of the excitation signal, and K is the curvature of the propagating wave, was used to estimate D. Measurements of N, c, and K were obtained directly from the data, with no dependence on modeling with cellular automata. J. P. Keener and J. J. Tyson, *Physica*, **21D**, 307 (1986).
14. P. H. Backx *et al.*, *J. Gen. Physiol.* **93**, 963 (1989).
15. M. Whitaker and R. F. Irvine, *Nature* **312**, 636 (1984).
16. P. Foerster, S. C. Muller, B. Hess, *Science* **241**, 685 (1988); *Proc. Natl. Acad. Sci. U.S.A.* **86**, 6831 (1989).
17. An auto-tracing routine (7) was used to define boundaries of equal intensity (>2 intensity units) along all spiral and spherical wavefront patterns of Ca^{2+} release for each optical slice. Regions outside these boundaries were not displayed in order to highlight the patterns of Ca^{2+} release over time. Only the brightest pixel is displayed along the observer's line of sight to add depth to the volume. The intensity scale refers to increases in $[Ca^{2+}]_i$ above resting.
18. We thank C. Bliton and the ANALYZE software support group (Mayo Foundation) for their assistance in imaging, C. Nanavati for assistance in computer modeling, and Dr. P. Camacho for reading the manuscript. Supported by the American Heart Association (J.L. and D.C.), by the Whitaker Foundation (D.C.), and by NIH (E.P. and D.C.).

9 November 1990; accepted 15 February 1991

Mediation of Responses to Calcium in Taste Cells by Modulation of a Potassium Conductance

ALBERTINO R. BIGIANI AND STEPHEN D. ROPER

Calcium salts are strong taste stimuli in vertebrate animals. However, the chemosensory transduction mechanisms for calcium are not known. In taste buds of *Necturus maculosus* (mud puppy), calcium evokes depolarizing receptor potentials by acting extracellularly on the apical ends of taste cells to block a resting potassium conductance. Therefore, divalent cations elicit receptor potentials in taste cells by modulating a potassium conductance rather than by permeating the cell membrane, the mechanism utilized by monovalent cations such as sodium and potassium ions.

RECEPTOR CELLS IN TASTE BUDS sense sodium, potassium, and calcium salts. The discovery that the chemosensitive surface of taste cells has a variety of ion channels has led to a greater understanding of how salts generate receptor potentials (*1*). For example, monovalent cations such as Na^+ and K^+ depolarize receptor cells by entering through specific ion channels in the apical membrane of taste cells (*2, 3*). However, it is still unclear how Ca^{2+} salts, which are powerful and commonly occurring taste stimuli (*4–6a*), are detected. Although voltage-gated Ca^{2+} channels are present in taste cells, they have a relatively high threshold for activation and would not be involved in chemosensory transduction unless taste cells were already depolarized by some other mechanism (*7, 8*).

We have taken advantage of the large taste cells in *Necturus maculosus* (mud puppy) to study chemotransduction mechanisms for Ca^{2+}. Earlier experiments have shown that the mud puppy can taste Ca^{2+} (*9, 10*). We therefore developed a slice preparation of the lingual epithelium (*11*) in which we could visualize and impale single taste cells in isolated living tissue and apply chemical stimuli to the taste pore. Lingual slices containing taste buds were placed in a recording chamber and perfused with amphibian physiological solution (APS) (*12*). Chemosensitivity was studied only in those taste cells that maintained stable resting potentials (−40 to −70 mV) and that responded with action potentials to brief depolarizing cur-

Department of Anatomy and Neurobiology, Colorado State University, Fort Collins, CO 80523, and the Rocky Mountain Taste and Smell Center, University of Colorado Health Sciences Center, Denver, CO 80262.

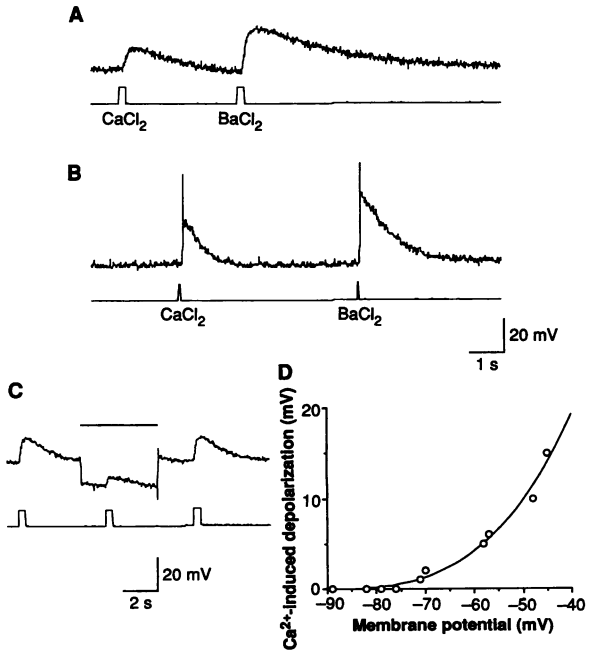

Fig. 1. (**A**) Taste cell responses to $CaCl_2$ and $BaCl_2$, focally applied to the taste pore (resting potential, −51 mV). (**B**) Responses in a different cell. If Ca^{2+} or Ba^{2+} responses were large enough, receptor potentials elicited action potentials (resting potential, −60 mV). Lower traces in (A) and (B) show the pulses of air pressure applied to the barrel of the micropipette containing the chemical stimulus. No responses were detected when the recording microelectrode was situated just outside the taste cell and chemical stimuli were applied. (**C**) Voltage dependence of the amplitude of the receptor potential induced by $CaCl_2$. Responses to $CaCl_2$ at resting potential (−45 mV), at a membrane potential of −58 mV established by passing dc current through the intracellular microelectrode (indicated by the horizontal bar), and again at resting potential. The lower trace monitors the application of $CaCl_2$. (**D**) Amplitude of $CaCl_2$ responses as a function of membrane potential [same cell as (C)]. Solid line, least-squares polynomial fit through the points. Intracellular recordings were obtained with glass micropipettes filled with 2.5 M KCl (90 to 180 megohms). An electrometer with a bridge circuit (WPI M4-A) was used to record the responses and to inject current into the taste cells. Signals were fed into a MacADIOS II GWI-625 data-acquisition board and processed with GWI SuperScope software.